High-Field EPR Study of Tyrosyl Radicals in Prostaglandin H_2 Synthase-1†

Pierre Dorlet,*,‡,§ Steve A. Seibold,‖,⊥ Gerald T. Babcock,‖ Gary J. Gerfen,# William L. Smith,⊥ Ah-lim Tsai,▽ and Sun Un§

Section de Bioénergétique, CNRS URA 2096, CEA Saclay, Bât. 532, 91191 Gif-sur-Yvette Cedex, France, Departments of Chemistry and Biochemistry, Michigan State University, East Lansing, Michigan 48824, Department of Internal Medicine, University of Texas Health Science Center at Houston, Houston, Texas 77225, and Albert Einstein College of Medicine, 1300 Morris Park Avenue, Bronx, New York 10461

Received October 19, 2001; Revised Manuscript Received March 11, 2002

ABSTRACT: Various tyrosyl radicals generated by reaction of both native and indomethacin-inhibited ovine prostaglandin H synthase-1 with ethyl hydrogen peroxide were examined by using high-field/high-frequency EPR spectroscopy. The spectra for the initially formed tyrosyl radical commonly referred to as the "wide-doublet" species and the subsequent "wide-singlet" species as well as the indomethacin-inhibited "narrow-singlet" species were recorded at several frequencies and analyzed. For all three species, the *g*-values were distributed. In the case of the wide doublet, the high-field EPR spectra indicated that dominant hyperfine coupling was likely to be also distributed. The g_x-values for all three radicals were found to be consistent with a hydrogen-bonded tyrosyl radical. In the case of the wide-doublet species, this finding is consistent with the known position of the radical and the crystallographic structure and is in contradiction with recent ENDOR measurements. The high-field EPR observations are consistent with the model in which the tyrosyl phenyl ring rotates with respect to both the protein backbone and the putative hydrogen bond donor during evolution from the wide-doublet to the wide-singlet species. The high-field spectra also indicated that the *g*-values of two types of narrow-singlet species, self-inactivated and indomethacin-inhibited, were likely to be different, raising the possibility that the site of the radical is different or that the binding of the inhibitor perturbs the electrostatic environment of the radical. The 130 GHz pulsed EPR experiments performed on the wide-doublet species indicated that the possible interaction between the radical and the oxoferryl heme species was very weak.

Prostaglandin H synthase (PGHS)[1] is a membrane-bound enzyme that exists as two isoforms, PGHS-1 and PGHS-2 (*1*). It is a key enzyme in the biosynthesis of prostaglandins and thromboxanes from arachidonic acid. It catalyzes the conversion of arachidonic acid into prostaglandin G_2 (cyclooxygenase) as well as the two-electron reduction of prostaglandin G_2 in prostaglandin PGH_2 (peroxidase). Thus the enzyme possesses both peroxidase and cyclooxygenase activity. The active site is distinct for each activity (*2*−*5*), but the cyclooxygenase reaction depends on the prior oxidation of the heme at the peroxidase active site. In the peroxidase cycle, the native state reacts with a peroxide species to form Compound I via a peroxy state. The so-called Intermediate II is composed of an oxoferryl entity on the heme together with a radical which has been shown to be located on tyrosine residue 385, and this radical initiates the cyclooxygenase cycle of the enzyme.

The crystallographic structure of oPGHS-1 has been determined (*3*) as well as the structures of the enzyme with bound arachidonic acid (*6*) or with bound inhibitors (*7*−*9*). In the peroxidase active site, located on the opposite side from the membrane-binding domain, the center of the heme is located about 12 Å from the phenoxyl oxygen of the Tyr385 residue which is at the edge of the cyclooxygenase active site constituted by a long hydrophobic channel where the substrate, as well as inhibitors such as indomethacin or aspirin, binds.

Several EPR signals of radicals have been reported in the studies of o-PGHS1 reactions. Mixing of oPGHS-1 with ethyl hydroperoxide in the presence of oxygen results in an initial formation of a radical species which exhibits a doublet line shape EPR signal, known as the wide doublet (WD), with a peak-to-trough width of about 33 G at 9 GHz (*10*, *11*). Upon incubation at 273 K, this signal rapidly evolves into a singlet line shape EPR signal with a similar width, the wide singlet (WS), before narrowing down to a 26 G wide singlet, the

† This work was supported by grants from the Human Frontiers Science Organization (Contract RGO349), from the EU through HCM grants FMRX-CT98-0214 and FMRX-CT96-0031, from the Région Ile-de-France (Contract Sésame) (P.D., S.U.), from PGG P01 GM57323 (W.L.S., S.A.S.), from NIH GM44911 (A.T.), from NIH GM60609 and NSF DBI-0096713 (G.J.G.). P.D. was supported by a fellowship from the CEA.

* To whom correspondence should be addressed: e-mail, pierre.dorlet@free.fr; telephone, +39 498275139; fax, +39 498275135.

‡ Present address: Dipartimento di Chimica Fisica, Università degli Studi di Padova, Via Loredan 2, 35131 Padova, Italy.

§ Section de Bioénergétique, CEA Saclay.

‖ Department of Chemistry, Michigan State University.

⊥ Department of Biochemistry, Michigan State University.

Albert Einstein College of Medicine.

▽ University of Texas Health Science Center at Houston.

[1] Abbreviations: C*c*P, cytochrome *c* peroxidase; CW, continuous wave; ENDOR, electron nuclear double resonance; EPR, electron paramagnetic resonance; EtOOH, ethyl hydroperoxide; HFEPR, high-field EPR; NS, narrow singlet; oPGHS-1, ovine PGHS-1; PGHS-1, prostaglandin endoperoxide H synthase-1; WD, wide doublet; WS, wide singlet.

10.1021/bi015871f CCC: $22.00
Published on Web 04/09/2002

self-inactivated narrow singlet (NS), upon longer incubation times (*12*). A narrow-singlet EPR signal, known as the inhibited narrow singlet, is also observed directly when the enzyme is pretreated with inhibitors of the cyclooxygenase activity (*13*). On the basis of deuterium labeling studies (*14*), it has been shown that all three species are tyrosine residues. The differences in the 9 GHz EPR experiments predominantly arise from differences in the electron−nuclear hyperfine coupling between the unpaired electron and the β protons.

An important issue is to determine whether all of these radicals correspond to the same site or to different ones. The wide-doublet species has been attributed to the Tyr385 residue after the results of chemical modification (nitration) (*15*) and mutagenesis studies (*14*). This residue has a prominent role in the rate-determining step in cyclooxygenase catalysis (see ref *16* and references cited therein). On the basis of results of computer simulations, DeGray and co-workers concluded that the WS was in fact a sum of the WD signal and the self-inactivated NS (*12*), but the relationship between the two narrow singlets, self-inactivated and inhibited, was not addressed. Tsai and co-workers (*17*, *18*) have suggested that the two types of NS correspond to distinct radicals. Experimental data supporting this fact were recently reported by Shi and co-workers using EPR and ENDOR spectroscopies (*19*). In this study, it was also concluded that the WS was in fact the sum of varying contributions of WD and self-inactivated NS spectra. On the basis of the absence of any detectable solvent-exchangeable protons, the ENDOR study of the WD species led to the conclusion that the radical responsible for this signal was not hydrogen-bonded (*19*).

Because tyrosyl radical *g*-values are sensitive probe of the environment of the radicals (*20*−*22*), we have used high-field EPR spectroscopy to further characterize the WD, WS, and indomethacin-inhibited NS. The spectra for these species were recorded at 190 and 285 GHz. Using such a multifrequency approach, it is possible to separate effects due to the *g*-values of the radical from those due to hyperfine interaction. The line shape of all three species spectra indicated that both *g*-tensor and hyperfine interaction parameters were distributed, in particular for the WD radical. The hydrogen-bonding status for the WD radical was analyzed in the light of the value measured for the g_x component and compared to the previous ENDOR and crystallographic studies. We also present pulsed EPR measurements performed at 130 GHz to study the possible magnetic interaction between the tyrosyl radical and the oxoferryl heme species.

MATERIALS AND METHODS

Sample Preparation. Ethyl hydroperoxide was purchased from Polyscience Inc. (Warrington, PA). Indomethacin and hemin were obtained from Sigma. oPGHS-1 was purified as described in ref *23*. For the CW EPR measurements, the WD tyrosyl radical sample was prepared by mixing the oPGHS-1 sample (30 μM in 50 mM HEPES buffer, pH 7, with 0.15% decyl maltoside) with a 2-fold excess of EtOOH directly in a 4 mm EPR tube, at 0 °C, and freeze-trapping in acetone/dry ice after 2 s. The WS tyrosyl radical sample was obtained by a thawing−freezing cycle of the WD sample. For the inhibited narrow singlet tyrosyl radical sample, oPGHS-1 was first exposed to indomethacin (40 μM in 50 mM HEPES buffer, pH 7, with 0.15% decyl maltoside), at 0 °C, for approximately 1 h and then reacted for 2 s with a 2-fold excess of ethyl hydroperoxide at 0 °C in an EPR tube before freezing in acetone/dry ice. Samples were stored in liquid nitrogen.

The samples used in the pulsed experiments were distinct from those used in the CW experiments for technical reasons and were prepared as previously described (*10*). After PGHS was mixed with EtOOH to initiate radical formation, the samples were drawn into 0.40 mm × 0.55 mm Suprasil quartz capillary tubes and frozen in liquid nitrogen. The total preparation time in this case was 6 s, after which time the 9 GHz spectrum still exhibited a predominant WD line shape. The samples were stored and loaded into the HFEPR probe under liquid nitrogen. The total active sample volume was approximately 125 nL.

EPR Spectroscopy. The 9 GHz EPR spectra were recorded with a TE_{102} cavity on a Bruker ESP300e spectrometer equipped with a liquid helium continuous-flow cryostat and transfer line from Oxford Instruments. The microwave frequency was measured with a Hewlett-Packard 5350B frequency counter connected to the microwave bridge. The 190 and 285 GHz EPR spectra were recorded on the transmission spectrometer built in Saclay, which is described elsewhere (*24*). The HFEPR spectra were recorded on the same samples used for the 9 GHz measurements.

The 130 GHz pulsed experiments were performed on a spectrometer assembled at Albert Einstein College of Medicine, which uses a bridge designed and built at the Donetsk Physico-Technical Institute of the Ukrainian National Academy of Sciences. It is a reflection spectrometer which employs a double-frequency conversion heterodyne detection scheme and cylindrical resonators operating in the TE_{011} mode. Typical $\pi/2$ pulse widths are 30−50 ns. The magnetic field is generated using a 7 T Magnex superconducting magnet equipped with a ±0.5 T sweep/active shielding coil. Temperature regulation of approximately ±0.3 K is achieved using an Oxford Spectrostat continuous-flow cryostat and ITC503 temperature controller.

Simulations of EPR Data. Second-order perturbation equations were used to calculate the spectrum. The high-field tyrosyl powder spectra were generated by calculating the resonant field for 10^6 random orientations of the applied magnetic field with respect to the *g*-axis frame and summing the results. The transition probability was taken to be unity. The resulting orientation-integrated spectra were convoluted with a derivative Gaussian function of suitable line width. Distributions in *g*-values were simulated by introducing a tensor, the principal values of which were collinear with the *g*-tensor of the radical. The principal values of the broadening tensor were the widths of Gaussian distributions along the three directions. Gaussian distributions were obtained by the method of normal deviates (*25*). The 190 and 285 GHz spectra were fitted simultaneously. All calculations were performed on a Digital Equipment Corp. workstation by using local programs written in Fortran 77.

RESULTS

Figures 1−3 show the HFEPR spectra of the so-called wide doublet (WD), wide singlet (WS), and indomethacin-

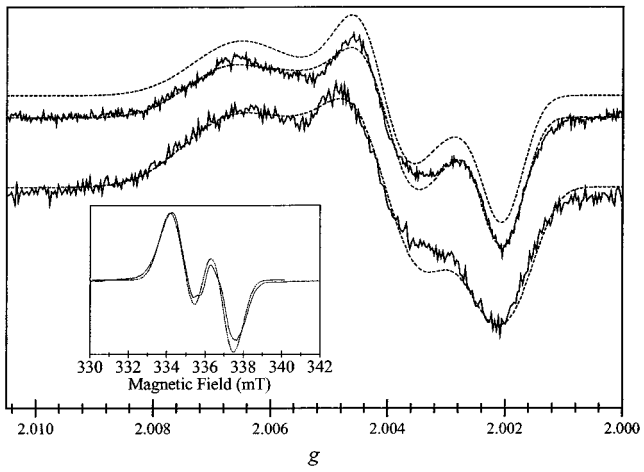

FIGURE 1: EPR spectra of the WD species generated by 2 s time reaction of PGHS-1 with EtOOH at 0 °C. Top spectra: 285 GHz. Bottom spectra: 190 GHz. Modulation amplitude: 20 G for both spectra. Solid line: experimental data. Dashed line: simulations. The top simulated spectrum has been calculated using the $S = 1$, $S = {}^1/_2$ interaction model (see text for details). Inset: 9 GHz spectrum recorded on the same sample used to record the HFEPR spectra at 190 and 285 GHz. Modulation amplitude: 3 G. Time constant: 41 ms. The parameters for the powder pattern simulations are listed in Table 1; the parameters for the $S = 1$, $S = {}^1/_2$ simulation are listed in Table 2.

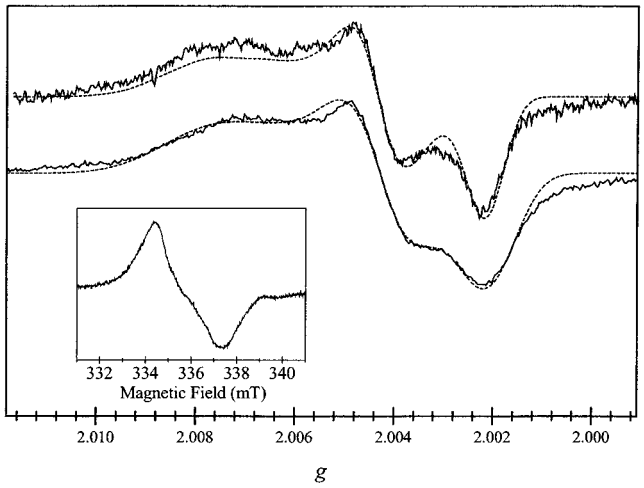

FIGURE 2: EPR spectra of the WS species obtained by incubation of the WD sample at 4 °C for 15 s. Top spectra: 285 GHz. Bottom spectra: 190 GHz. Modulation amplitude: 20 G for both spectra. Inset: 9 GHz spectrum. Modulation amplitude: 3 G. Time constant: 164 ms. All spectra have been recorded on the same sample. Solid line: experimental data. Dashed line: simulations. The parameters for the simulations are listed in Table 1.

inhibited narrow singlet (NS), respectively. In each case, the corresponding 9 GHz spectrum of the same sample is shown in the inset. The WD sample was generated by reacting oPGHS-1 with a 2-fold excess of EtOOH for 2 s at 0 °C. The 9 GHz WD spectrum (Figure 1, inset) exhibited the usual wide-doublet line shape with a peak-to-trough splitting of 33 G (*13*, *26*). This doublet structure is due to the hyperfine coupling of one of the β-methylene protons (see Scheme 1). The WS sample was obtained by incubation of the WD sample at 4 °C for 15 s. The 9 GHz WS spectrum (Figure 2, inset) is characterized by a singlet-like spectrum with a peak-to-rough width of 30 G. Reaction of indomethacin-treated oPGHS-1 samples with ethyl hydroperoxide directly yielded

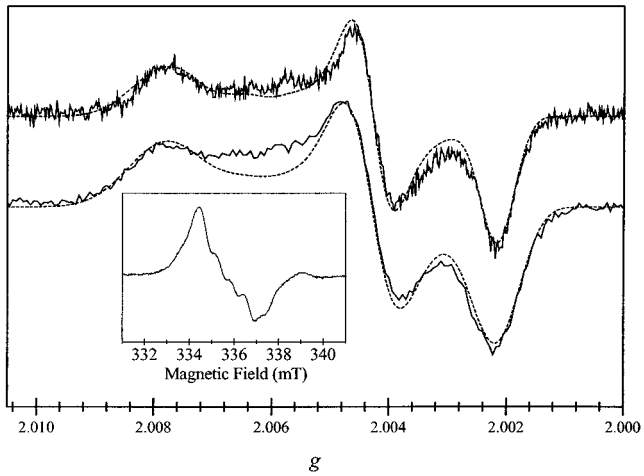

FIGURE 3: EPR spectra of the indomethacin-inhibited NS species obtained by reaction of indomethacin-treated PGHS-1 with EtOOH for 2 s. Top spectra: 285 GHz. Bottom spectra: 190 GHz. Modulation amplitude: 20 G for both spectra. Inset: 9 GHz spectrum. Modulation amplitude: 3 G. Time constant: 82 ms. All spectra have been recorded on the same sample. Solid line: experimental data. Dashed line: simulations. The parameters for the simulations are listed in Table 1.

samples with a 9 GHz singlet-like line shape with a narrower peak-to-trough width of 25 G.

At 285 GHz and 10 T, the HFEPR spectra (Figures 1−3, upper traces) of the three types of samples were clearly different from the corresponding 9 GHz spectra. The overall spectra width ranged from about 230 to 290 G; the NS spectrum was broader than the WD. As expected from theory, the high-field edge of the spectra corresponding to the g_z-value was slightly lower than the free electron g-value of 2.00232 (*27*). The low-field edge corresponding to the g_x-value differed with the following order: g_x(NS) > g_x(WS) > g_x(WD). The indomethacin-inhibited NS g_x-value (2.0078) was similar to that of the tyrosine D radical in photosystem II (2.00756), and the WD value (2.0068) was similar to that of the tyrosyl radical in tyrosine HCl crystals (2.00658). In all three cases, the hyperfine structure could not be resolved, and the spectra were broadened to an extent that could not be accounted for solely by unresolved hyperfine couplings. To clarify the relative contributions to inhomogeneous line widths, we obtained spectra at 190 GHz.

Hyperfine interactions, which dominate the 9 GHz PGHS spectra, are to first order independent of the applied magnetic field. By comparison, the Zeeman interaction is directly proportional to the applied magnetic field. Therefore, by recording the HFEPR spectra at two different frequencies, it is possible to separate the contributions from hyperfine and Zeeman interactions. This is visually accomplished by plotting the multifrequency data as a function of g-values rather than magnetic field. When plotted in this manner, the line widths of the features that are dominated by hyperfine couplings will have an inverse relationship to the microwave frequency and those dominated by Zeeman interaction will be frequency independent. Figures 1−3 show the 190 and 285 GHz spectra of the WD, WS, and inhibited NS samples plotted as a function of g-values.

The overall frequency dependence of the HFEPR spectra of the three types of samples was approximately the same. In each case, the g_z-edge (high-field edge) of the 190 GHz

Scheme 1

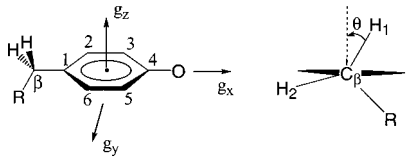

Tyrosyl radical numbering and g-tensor orientation

C_β-H_1 dihedral angle

Table 1: Parameters Used for the Simulations of the Spectra

	wide doublet	130 GHz pulsed EPR spectrum	wide singlet	inhibited narrow singlet
g_x (σ_x)[a]	2.0068 (0.0007)	2.0070 (0.0007)	2.0078 (0.0009)	2.0078 (0.0005)
g_y (σ_y)	2.0040 (0.0003)	2.0041 (0.0004)	2.0043 (0.0003)	2.0043 (0.0001)
g_z	2.0020	2.0021	2.0021	2.0021
$H_{3,5}$ A_x[b]	26	26	26	26
$H_{3,5}$ A_y	7	7	7	7
$H_{3,5}$ A_z	19	19	19	19
H_β A_x	51	51	45	27
H_β A_y	51	51	45	27
H_β A_z	52	52	50	33

[a] σ_i is the half-width at half-maximum of the Gaussian distribution about g_i. [b] Absolute values for hyperfine coupling constants are given in megahertz.

spectrum was clearly broader than the 285 GHz spectra, indicating that the line width at this principal *g*-value was predominated by hyperfine interaction. By comparison, the line width of the g_x-edge was approximately frequency independent, indicating the dominance of the Zeeman interaction. The large central g_y-features exhibited an intermediate behavior. To quantify further these effects, simulations were carried out.

In the simulations, the hyperfine coupling parameters in the fitting procedure were fixed. The values for the ring protons (see Scheme 1 for numbering), which are approximately the same for all tyrosyl radicals (*28*), were taken from the literature (*19*). In the case of the WD spectra, the values for the β protons, which are known to be largely isotropic (*29*), were then adjusted and fixed to account for the line width of the g_z-edge. The values obtained for the strongly coupled β proton were significantly smaller than those measured by ENDOR at 9 GHz (*19*) (see below). However, the parameters from the HFEPR spectra gave a satisfactory simulation of the 9 GHz spectrum (see Figure 1 insert). By contrast, the HFEPR line widths of the WS and NS spectra were completely consistent with the hyperfine values obtained from 9 GHz simulations (*19*), and those values were used for the HFEPR data simulations. As discussed above, the large width of the g_x- and g_y-features could not be accounted for solely by hyperfine interactions, and distributions in the g_x- and g_y-values were necessary to simulate the experimental data. The variable parameters in the fitting procedure were the three *g*-values and the three widths of the Gaussian distribution about these values. The 190 and 285 GHz spectra were fitted simultaneously. The *g*-values and distributions obtained from the best fits of the experimental data are listed in Table 1. The calculated HFEPR spectra are plotted in Figure 1 along with the experimental data.

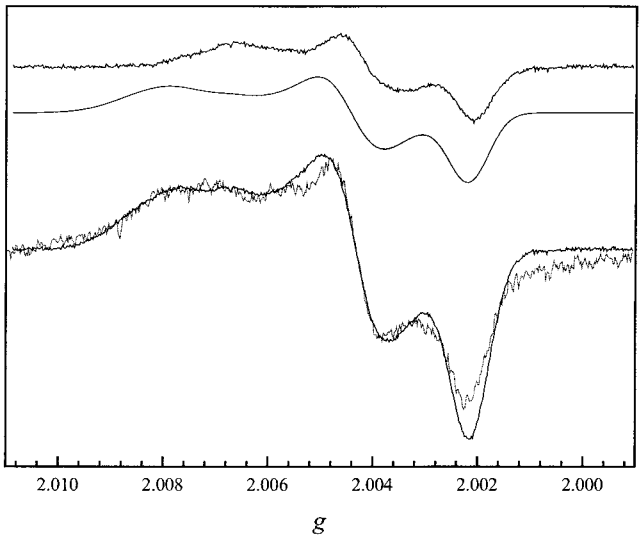

FIGURE 4: Decomposition of the WS 285 GHz HFEPR spectrum into the WD and NS spectra. From top to bottom: WD spectrum, simulated NS powder spectrum {parameters: g = [2.0080 (0.0007), 2.0040 (0.0004), 2.0021], $A_{3,5}$ = (26, 7, 20) MHz, A_β = (34, 34, 36) MHz}, sum (black) of WD and simulated NS spectra superimposed on the WS spectrum (gray). The parameters used for the NS simulation are different from those obtained from the indomethacin-inhibited NS spectra (see Figure 3, Table 1, and text for details).

The line width of the HFEPR features in the indomethacin-inhibited NS spectrum is narrower compared to the WD species, and a smaller distribution was required in order to fit the spectra. The g_x-value for the inhibited NS sample was noticeably higher at 2.0078 than the WD species g_x-value of 2.0068. The WS sample presented an intermediate case with respect to the *g*-values and the distribution in g_x- and g_y-values. An alternate approach to simulating the high-field WS spectra was an extension of the original proposal by DeGray and co-workers (*12*) for simulating the 9 GHz WS spectrum: a weighted sum of the spectra corresponding to the WD species and the self-inactivated NS species. This approach considers the WS spectrum to arise from a mixture of the WD and the self-inactivated NS species rather than corresponding to a distinct tyrosyl radical. The ENDOR study of Shi and co-workers (*19*) has provided evidence supporting this view. It is clear from the HFEPR data that the WS cannot be a mixture of WD and indomethacin-inhibited NS. The range of the WS g_x-values not only covers the entire range of both the WD and indomethacin-inhibited NS values but also significantly extends to higher *g*-values. Therefore, if the WS is indeed the sum of the WD and self-inactivated NS spectra, then the g_x-values for the two types of NS must be different. Minimally, the extent of the g_x-edge of the self-inactivated tyrosyl radical must be higher than that of the indomethacin-inhibited NS. The loss of the tyrosyl radical signal amplitude upon further incubation of the sample on ice did not allow us to record the HFEPR spectra on the self-inactivated NS radical. However, it was possible to simulate the WS HFEPR spectra by combining the WD signal with a second spectrum which had a different set of *g*-values from that of the indomethacin-inhibited NS spectrum (see Figure 4). The differences in NS *g*-values suggest either that the two radicals are on different sites, supporting the conclusion of the earlier ENDOR study (*19*), or that the

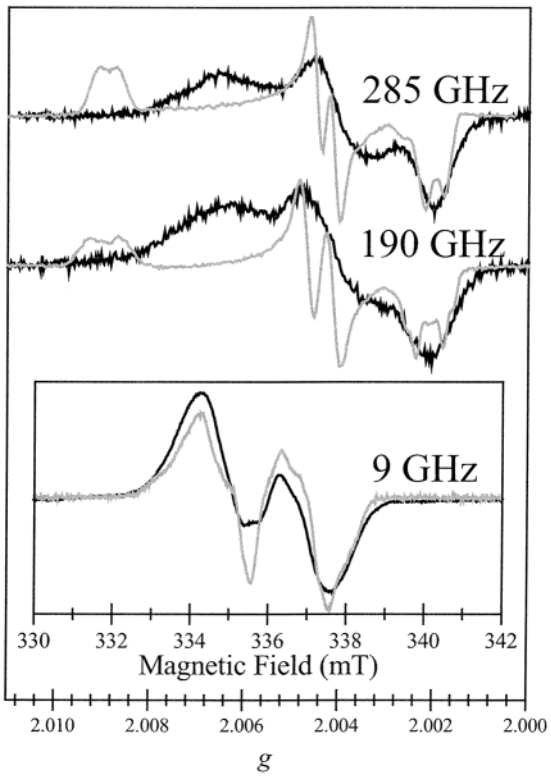

FIGURE 5: EPR spectra of the WD tyrosyl radical in oPGHS-1 (black line) and of the tyrosyl radical in RNR (gray line). Spectra of the WD are as in Figure 1. The resolution of the WD spectra was unaffected by the use of a low modulation amplitude. In each case, all spectra have been recorded on the same sample.

radical site is the same but that the binding of indomethacin greatly affects the electrostatic environment of the residue (*20*, *21*).

The evolution from the WD to the self-inactivated NS-type spectra observed at 9 GHz clearly involves changes in hyperfine couplings. However, the changes in the g_x-region of the HFEPR spectra cannot be explained only by changes in hyperfine interactions. Hence, the underlying molecular mechanism for the spectral evolution manifests itself differently in conventional and high-field EPR spectra: at 9 GHz, changes in hyperfine couplings are the dominant features whereas changes in the *g*-values dominate in the HFEPR data.

The WD hyperfine values obtained for the strongly coupled β-methylene proton measured by ENDOR are similar to those of the RNR tyrosyl radical. Consequently, the 9 GHz spectra of both radicals are similar (see Figure 5). However, in the HFEPR spectra, the resolved features at the g_z-edge observed in the RNR spectra due to this hyperfine interaction are absent in the WD spectra. The 190 and 285 GHz data clearly show that the apparently lower resolution of the WD spectrum is due to field-independent interactions and not to distributions in *g*-values (see Figure 1). A likely explanation is that the dominant β-coupling hyperfine interaction is itself distributed. This would explain why the 9 GHz WD spectrum appears slightly less resolved than the RNR spectrum, yet having the same apparent couplings, and why hyperfine values obtained from HFEPR simulations were smaller than those measured by ENDOR.

To study a possible interaction between the tyrosyl radical and the oxoferryl species and determine if it could influence

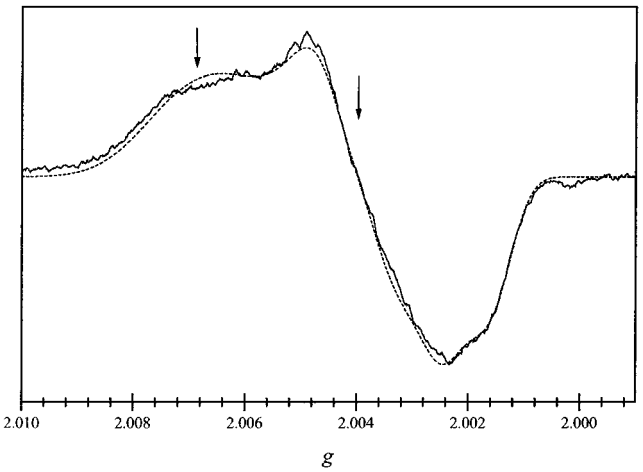

FIGURE 6: 130 GHz Hahn echo-detected EPR spectrum of a 6 s quench oPGHS-1 sample reacted with EtOOH. The numerical derivative of the acquired echo-detected EPR spectrum is presented. The arrows indicate positions at which the pulsed saturation−recovery curves presented in Figure 7 were recorded. Data acquisition parameters were as follows: temperature, 6.0 K; pulse 1 width, 30 ns; pulse 2 width, 60 ns; time between pulses, 150 ns.

the spectral positions and shapes in the EPR spectra, we measured pulsed HF (130 GHz) EPR saturation−recovery curves under conditions which could be compared with well-characterized tyrosyl radical species in ribonucleotide reductase (RNR) systems (*20*, *30*−*33*). Figure 6 shows the echo-detected field sweep EPR signal obtained at 130 GHz on a 6 s quench sample of oPGHS-1 reacted with EtOOH. The simulation of the spectrum is shown along with experimental data. Simulation parameters are reported in Table 1. Figure 7 shows the 130 GHz pulsed saturation−recovery curves measured at 5.8 K and at field positions corresponding to g_x and g_y, respectively. Monoexponential and biexponential fits of the experimental curves are also shown in the figures.

DISCUSSION

In a series of studies, it has been demonstrated that the *g*-values of tyrosyl radicals are sensitive to the local electrostatic environment (*20*−*22*). Crystallographic (*7*) and mutagenesis (*14*) data show that the likely site of the WD tyrosyl radical, Tyr385, is hydrogen-bonded (see below). The range of g_x-values found for the PGHS radical(s) is consistent with an electropositive environment due to one or more hydrogen bonds. Furthermore, our HFEPR results indicate that the progression from the WD to the self-inactivated NS-type radical, as observed by conventional 9 GHz EPR spectroscopy, is paralleled by a change from a strongly to moderately hydrogen-bonded tyrosyl radical. HFEPR spectroscopy cannot unambiguously distinguish whether this evolution occurs on a single tyrosyl radical or through a migration of the unpaired spin to one or a series of tyrosyl residues. Because all three types of HFEPR spectra exhibit a g_x-edge that is continuously rather than discretely distributed and because of the contiguous change of the g_x-edge during incubation of a single sample, we favor the single site model for the radical. Indeed, the explanation of these two observations in the context of a migration mechanism would require sequential tyrosine sites with progressively weaker distributed hydrogen bonds, which seems unlikely.

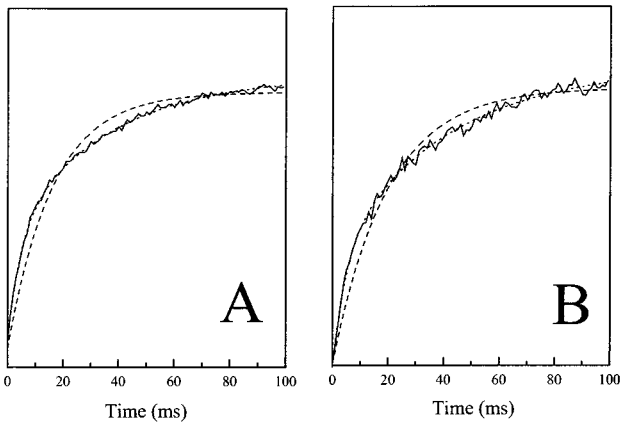

FIGURE 7: 130 GHz pulsed saturation−recovery curves of a 6 s quench oPGHS-1 sample reacted with EtOOH. Panel A: The experimental curve (solid line) was obtained at a field position corresponding to approximately g_x (4.6295 T). The dotted curve is the best biexponential fit with $1/T_a = 211$ s^{-1} and $1/T_b = 25$ s^{-1}. The dashed curve is the best monoexponential fit with $1/T_1 = 51$ s^{-1}. Panel B: The experimental curve (solid line) was obtained at a field position corresponding to approximately g_y (4.6558 T). The dotted curve is the best biexponential fit with $1/T_a = 219$ s^{-1} and $1/T_b = 29$ s^{-1}. The dashed curve is the best monoexponential fit with $1/T_1 = 62$ s^{-1}. Data acquisition parameters for both curves were as follows: temperature, 5.8 K; saturating pulse, 60 ms; Hahn echo detection, pulse 1 = 30 ns, pulse 2 = 60 ns, and $\tau = 150$ ns; repetition rate, 5 Hz; 300 averages per point.

By contrast, an evolution in hydrogen bonding for a single site is consistent with the phenyl ring rotational model that has been developed to rationalize the evolution of the 9 GHz EPR spectra. The strength of a hydrogen bond critically depends on both the distance and angular orientation between the donor and acceptor. Hence a rotation of the tyrosyl radical acceptor relative to the donor will modulate the strength of the hydrogen bond (*34*). A potential driving force for such a rotation is the energy difference between hydrogen bonding in the reduced and oxidized species. The hydrogen-bonding energy and geometry of the two redox states are unlikely to be the same. Hence, upon oxidation, rearrangement of the hydrogen-bonding geometry is expected.

A refined 2.7 Å resolution structure of the PGHS synthase has been published recently (*7*). It shows that Tyr385, the proposed site of the radical, is in very close proximity to another tyrosine residue (Tyr348) with a phenolic oxygen−oxygen distance of 2.78 Å, as well as to a water molecule with an oxygen−oxygen distance of 2.77 Å (see Figure 8), indicating the presence of two relatively strong hydrogen bonds to the radical site. Yet, in their ENDOR study, Shi and co-workers did not detect any exchangeable proton that could be associated with a hydrogen bond in the WD sample, and it was therefore concluded that the tyrosyl radical responsible for the WD signal was not hydrogen-bonded. An argument invoked to support this result was the g_x-value obtained from simulations of the 9 GHz data which yielded a value of 2.0089. Now that this value has been measured with HFEPR, this argument no longer holds and actually points toward the opposite result. Given the large distribution of the g_x-value required to properly fit the HFEPR data, it is likely that any proton ENDOR resonance associated with hydrogen bonds to the phenolic oxygen of Tyr385 would be obscured in the ENDOR spectrum. Such a situation has been previously encountered. In contrast to the tyrosyl D

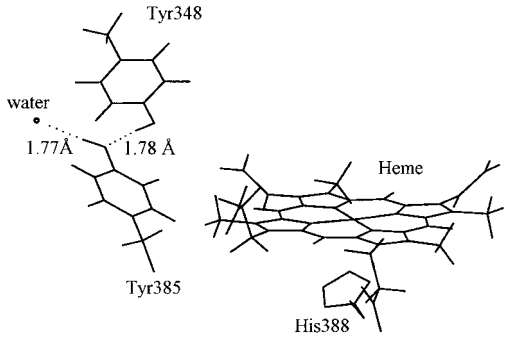

FIGURE 8: Structure of the peroxidase active site of o-PGHS-1 based on the 2.70 Å resolution crystallographic structure of the enzyme complexed with flurbiprofen. To emphasize possible hydrogen bonds involving the tyrosine 385 residue, standard hydrogen atoms were added to the PDB file by using the program Reduce (*46*). Distances given are oxygen−hydrogen distances. The figure was generated by using the programs Prekin and Mage (*47*).

Table 2: Parameters Used for the Simulation of the 285 GHz WD Spectrum with the $S = 1$, $S = {}^1/_2$ Model

	x	*y*	*z*
tyrosine *g*-values	2.0075	2.0043	2.0021
Fe species *g*-values	2.0012	2.0012	2.0012
interaction tensor (GHz)[a]	0.140 (0.150)	0.015 (0.060)	
zero-field splitting parameters (GHz)	$D = 660$	$E = 0$	

[a] See ref *38* for details on the model. The value in parentheses represents the half-width at half-maximum of a Gaussian distribution.

radical in photosystem II, ENDOR measurements of the tyrosyl Z radical provided no evidence of a hydrogen bond (no ^2H_2O exchangeable features could be detected by CW-ENDOR) (*35*), yet the *g*-values of both photosystem II radicals measured by HFEPR were nearly identical (*34*). The key difference between the radicals was a distribution in the g_x-value of the tyrosyl Z radical. The ^2H pulsed ENDOR study also indicated the presence of a hydrogen bond which was distributed (*36*). In the presence of a distributed hydrogen bond, what is observed in the ENDOR experiment could be complicated: some resonances may be broadened beyond detection, and the apparent position of the turning points may be distorted due to the distribution in the position of the radical. In addition, the pocket which constitutes the cyclooxygenase active site in oPGHS-1 is hydrophobic. The crystal structure reveals fewer water molecules in this area, implying a slow solvent exchange rate and thus prohibiting significant changes in proton ENDOR experiments.

Apart from hydrogen bonding, another cause for the low g_x-value of the WD could be a magnetic interaction with the $S = 1$ heme iron species. It has been shown in the case of C*c*P Compound ES (*37*, *38*) that an interaction between the $S = 1$ oxoferryl moiety and a $S = {}^1/_2$ radical results in a line shape that is powder pattern-like with effective *g*-values that depend on the *g*-values for the uncoupled radical corrected by a term proportional to the ratio of the coupling parameter by the zero-field splitting parameter of the iron species. Therefore, a weakly hydrogen-bonded tyrosyl radical coupled to the oxoferryl species could have *g*-values such as those measured for the WD species in this study (see Figure 1 and Table 2; it must be noted that no hyperfine interaction is implemented in this specific simulation program; therefore, the broadening of the spectra was accounted

for by a distribution of the coupling parameters). In the case of C*c*P Compound ES, the tryptophanyl radical is coupled to the oxoferryl iron moiety with a distance between the radical indole nitrogen and the iron ion of 7.1 Å as measured from the crystallographic structure. In the case of PGHS, the distance between the Tyr385 phenolic oxygen and the iron ion is 12.5 Å. Since the dipolar and exchange couplings decrease with increasing distance between the interacting species (*39*, *40*), the interaction is expected to be much weaker for PGHS compared to C*c*P. At a distance of 12.5 Å, the corresponding dipolar coupling, using a point−dipole model, is −27 MHz ($\delta = -\mu^0 g^2 \beta^2 / 4\pi r^3$). Simulations of the 285 GHz WD spectrum with the $S = 1$, $S = {}^1/_2$ interaction model, with an intrinsic g_x-value of 2.0075 for the radical, led to isotropic and dipolar spin-coupling parameters that were below 100 MHz. Therefore, a very weak spin-coupling effect is consistent with the observed broadening. A rotation of the side chain of the tyrosine would modify orbital overlaps, and hence exchange interactions, leading to further weakening of the coupling and increase of the g_x-value.

Further information on a possible weak coupling between the oxoferryl center and the tyrosyl radical was obtained from high-frequency pulsed saturation−recovery experiments. Previous CW X-band power saturation studies on the PGHS doublet and singlet species produced evidence for an interaction with the oxoferryl center (*11*, *41*). RNR systems provide meaningful comparisons with the PGHS case because the effects of the diferric metal center which produces the relaxation enhancement of the tyrosyl radical can be controlled by temperature: at low temperatures, the paramagnetic $S = 1$ state of the antiferromagnetically coupled diiron center is significantly depopulated and the tyrosyl radical relaxes near its "intrinsic" (noninteracting) rate; at higher temperatures, the $S = 1$ state of the metal center becomes populated and increases the relaxation rate of the nearby tyrosyl radical through exchange and dipolar interactions.

The pulsed saturation−recovery curves were measured at 5.8 K and 130 GHz. At this frequency and temperature, the data can be compared to a recent pulsed HFEPR study of *Escherichia coli* and yeast RNR tyrosyl radicals (*33*). This study found that, below 10 K, the RNR tyrosyl radical saturation−recovery curves exhibited multiexponential behavior which, if best-fit with a single exponential function to give a $1/T_1$ estimate, exhibited approximately 25% anisotropy in rates across the EPR spectrum. As is clear from the fits presented in Figure 7, both curves obtained from PHGS are best described as at least biexponential, with an anisotropy in the best-fit monoexpontial $1/T_1$ values of 20% between g_x and g_y excitation positions. In addition, the best-fit monoexponential $1/T_1$ values measured for PGHS (62 and 51 s^{-1}at 6 K) are in the range of those reported for RNR systems at approximately the same temperature (30−70 s^{-1} at 8 K). Because the RNR tyrosyl radical experiences a reduced influence on its relaxation behavior from the diferric iron center at these temperatures (*30*−*32*), the similarity of the PGHS tyrosyl radical relaxation behavior to that in the RNR systems suggests that the coupling of the PGHS tyrosyl radical to the oxoferryl center is correspondingly small.

It must be noted that comparisons of the CW saturation behavior of the *E. coli* RNR tyrosyl radical with PSII Y_D at 245 GHz indicate that the relaxation behavior of the RNR tyrosyl radical at low and high EPR frequency/field may differ (*20*). At 4.5 K, the high-frequency RNR tyrosyl spectrum required higher microwave powers for saturation than Y_D with PSII in the diamagnetic S_1 state, suggesting that either the intrinsic relaxation properties of the radicals differ at high field or the RNR tyrosyl radical experiences an interaction with the diferric center which can be more readily detected at high field. However, at this temperature, the peak positions and line widths of RNR tyrosyl radical EPR spectra acquired at 9 GHz (*30*), 140 GHz (*42*), and 245 GHz (*20*) are not affected by the interaction with the diferric iron center: the spectra can be well simulated as isolated tyrosyl radicals without using electron−electron interactions. Because the small metal−radical interaction present in RNR at these temperatures does not perturb the EPR spectra to any observable extent, and because the relaxation properties of the PGHS radical have been shown to be similar to those of RNR, it is reasonable to conclude that the PGHS spectra are not significantly influenced by coupling to the oxoferryl center. These relaxation results indicate that the g_x-value and broadening of the WD species are dominated by hydrogen bonding rather than spin−spin interaction with the oxyferryl state.

The oxoferryl species is also an $S = 1$ species with an $S = 0$ ground state. However, the zero-field splitting of this species is smaller than that for the diferric center in RNR, and the $S = 1$ state is significantly populated even at temperatures below 4.2 K. For example, in C*c*P Compound ES at 4.2 K, the relaxation rates of the coupled tryptophan radical are increased by 2−3 orders of magnitude over those expected for an isolated organic radical (*37*). As discussed previously, the EPR spectrum of this tryptophan radical is strongly perturbed by the coupling to the iron center. However, the relaxation rates measured for the PGHS radical indicate a much smaller interaction (and thus an Fe−tyrosyl distance significantly greater than the Fe−tryptophan distance of C*c*P Compound ES) which has a negligible influence on the EPR spectrum.

In summary, the HFEPR data indicate that the WD tyrosyl radical is hydrogen-bonded. However, the hydrogen bonding is distributed, and the electrostatic effect of the hydrogen bond appears to change over time, suggesting that the radical is initially in a strained environment. This change in hydrogen bonding is consistent with the rotation of the phenyl ring with respect to the protein backbone, which would necessarily change the relative orientation of the hydrogen bond donor and, therefore, the hydrogen-bonding energy. It is known from studies of tyrosyl radicals in proteins and model systems that local electrostatic effects, such as hydrogen bonds, can strongly modify the stability and redox properties of the tyrosyl radical (*43*−*45*). In the case of PGHS, mutagenesis experiments indicate that Tyr348, one of the likely hydrogen bond donors to the tyrosyl radical, is not essential for cyclooxygenase activity. However, it has been argued that Tyr348 may play a structural role in positioning the substrate relative to Tyr385 (*6*). Consistent with both the mutagenesis and HFEPR studies is the possibility that the Tyr348 through the hydrogen-bonding interaction induces a reorientation of the radical to promote the hydrogen abstraction from the substrate. Clearly, further HFEPR studies on mutants are required to test this hypothesis.

ACKNOWLEDGMENT

This work was initiated and done in collaboration with Prof. Jerry Babcock and is dedicated to his memory. We thank Dr. Richard J. Kulmacz and Graham Palmer for help in earlier preliminary results. P.D. and S.U. thank Bill Rutherford and Anabella Ivancich for encouragement and discussions and Guillaume Voyard for technical assistance. We also thank Rajendra Bose Muthukumaran for preliminary checking with 9 GHz EPR the samples used for CW EPR measurements. G.J.G. thanks Vladimir Krymov for technical assistance in the acquisition of the 130 GHz data.

REFERENCES

1. Smith, W. L., Garavito, R. M., and DeWitt, D. L. (2000) *Annu. Rev. Biochem. 69*, 145−182.
2. Marshall, P. J., and Kulmacz, R. J. (1988) *Arch. Biochem. Biophys. 266*, 162−170.
3. Picot, D., Loll, P. J., and Garavito, R. M. (1994) *Nature 367*, 243−249.
4. Kurumbail, R. G., Stevens, A. M., Gierse, J. K., McDonald, J. J., Stegeman, R. A., Pak, J. Y., Gildehaus, D., Miyashiro, J. M., Penning, T. D., Seibert, K., Isakson, P. C., and Stallings, W. C. (1996) *Nature 384*, 644−648.
5. Luong, C., Miller, A., Barnett, J., Chow, J., Ramesha, C., and Browner, M. F. (1996) *Nat. Struct. Biol. 3*, 927−933.
6. Malkowski, M. G., Ginell, S. L., Smith, W. L., and Garavito, R. M. (2000) *Science 289*, 1933−1937.
7. Selinsky, B. S., Gupta, K., Sharkey, C. T., and Loll, P. J. (2001) *Biochemistry 40*, 5172−5180.
8. Loll, P. J., Picot, D., Ekabo, O., and Garavito, R. M. (1996) *Biochemistry 35*, 7330−7340.
9. Loll, P. J., Picot, D., and Garavito, R. M. (1995) *Nat. Struct. Biol. 2*, 637−643.
10. Kulmacz, R. J., Tsai, A.-L., and Palmer, G. (1987) *J. Biol. Chem. 262*, 10524−10531.
11. Karthein, R., Dietz, R., Nastainczyk, W., and Ruf, H. H. (1988) *Eur. J. Biochem. 171*, 313−320.
12. DeGray, J. A., Lassmann, G., Curtis, J. F., Kennedy, T. A., Marnett, L. J., Eling, T. E., and Mason, R. P. (1992) *J. Biol. Chem. 267*, 23583−23588.
13. Kulmacz, R. J., Ren, Y., Tsai, A.-L., and Palmer, G. (1990) *Biochemistry 29*, 8760−8771.
14. Tsai, A.-L., Hsi, L. C., Kulmacz, R. J., Palmer, G., and Smith, W. L. (1994) *J. Biol. Chem. 269*, 5085−5091.
15. Shimokawa, T., Kulmacz, R. J., DeWitt, D. L., and Smith, W. L. (1990) *J. Biol. Chem. 265*, 20073−20076.
16. Smith, W. L., DeWitt, D. L., and Garavito, R. M. (2000) *Annu. Rev. Biochem. 69*, 145−182.
17. Tsai, A.-L., Kulmacz, R. J., and Palmer, G. (1995) *J. Biol. Chem. 270*, 10503−10508.
18. Tsai, A.-L., and Kulmacz, R. J. (2001) *Prostaglandins Other Lipid Mediators 62*, 231−254.
19. Shi, W., Hoganson, C. W., Espe, M., Bender, C. J., Babcock, G. T., Palmer, G., Kulmacz, R. J., and Tsai, A.-L. (2000) *Biochemistry 39*, 4112−4121.
20. Un, S., Atta, M., Fontecave, M., and Rutherford, A. W. (1995) *J. Am. Chem. Soc. 117*, 10713−10719.
21. Un, S., Gerez, C., Elleingand, E., and Fontecave, M. (2001) *J. Am. Chem. Soc. 123*, 3048−3054.
22. Ivancich, A., Mattioli, T. A., and Un, S. (1999) *J. Am. Chem. Soc. 121*, 5743−5753.
23. Seibold, S. A., Cerda, J. F., Mulichak, A. M., Song, I., Garavito, R. M., Arakawa, T., Smith, W. L., and Babcock, G. T. (2000) *Biochemistry 39*, 6616−6624.
24. Dorlet, P., Rutherford, A. W., and Un, S. (2000) *Biochemistry 39*, 7826−7834.
25. Press, W. H., Flannery, B. P., Teukolsky, S. A., and Vetterling, W. T. (1986) *Numerical Recipes*, Cambridge University Press, New York.
26. Tsai, A.-L., Palmer, G., and Kulmacz, R. J. (1992) *J. Biol. Chem. 267*, 17753−17759.
27. Angstl, R. (1989) *Chem. Phys. 132*, 435−442.
28. Babcock, G. T., Espe, M., Hoganson, C., LydakisSimantiris, N., McCracken, J., Shi, W. J., Styring, S., Tommos, C., and Warncke, K. (1997) *Acta Chem. Scand. 51*, 533−540.
29. Hoganson, C. W., and Babcock, G. T. (1992) *Biochemistry 31*, 11874−11880.
30. Sahlin, M., Petersson, L., Gräslund, A., Ehrenberg, A., Sjöberg, B.-M., and Thelander, L. (1987) *Biochemistry 26*, 5541−5548.
31. Hirsh, D. J., Beck, W. F., Lynch, J. B., Que, L. J., and Brudvig, G. W. (1992) *J. Am. Chem. Soc. 114*, 7475−7481.
32. Galli, C., Atta, M., Andersson, K. K., Gräslund, A., and Brudvig, G. W. (1995) *J. Am. Chem. Soc. 117*, 740−746.
33. Bar, G., Bennati, M., Nguyen, H.-H. T., Ge, J., Stubbe, J., and Griffin, R. G. (2001) *J. Am. Chem. Soc. 123*, 3569−3576.
34. Un, S., Tang, X. S., and Diner, B. A. (1996) *Biochemistry 35*, 679−684.
35. Tommos, C., Tang, X. S., Warncke, K., Hoganson, C. W., Styring, S., McCracken, J., Diner, B. A., and Babcock, G. T. (1995) *J. Am. Chem. Soc. 117*, 10325−10335.
36. Force, D. A., Randall, D. W., Britt, R. D., Tang, X. S., and Diner, B. A. (1995) *J. Am. Chem. Soc. 117*, 12643−12644.
37. Houseman, A. L., Doan, P. E., Goodin, D. B., and Hoffman, B. M. (1993) *Biochemistry 32*, 4430−4443.
38. Ivancich, A., Dorlet, P., Goodin, D. B., and Un, S. (2001) *J. Am. Chem. Soc. 123*, 5050−5058.
39. Coffman, R. E., and Buettner, G. R. (1979) *J. Phys. Chem. 83*, 2387−2392.
40. Abragam, A., and Bleaney, B. (1970) *Electron Paramagnetic Resonance of Transition Ions*, Clarendon, Oxford, U.K.
41. Lassmann, G., Odenwaller, R., Curtis, J. F., DeGray, J. A., Mason, R. P., Marnett, L. J., and Eling, T. E. (1991) *J. Biol. Chem. 266*, 20045−20055.
42. Gerfen, G. J., Bellew, B. F., Un, S., Bollinger, J. M., Jr., Stubbe, J., Griffin, R. G., and Singel, D. J. (1993) *J. Am. Chem. Soc. 115*, 6420−6421.
43. Thuresson, E. D., Lakkides, K. M., Rieke, C. J., Sun, Y., Wingerd, B. A., Micielli, R., Mulichak, A. M., Malkowski, M. G., Garavito, R. M., and Smith, W. L. (2001) *J. Biol. Chem. 276*, 10347−10357.
44. Word, J. M., Lovell, S. C., Richardson, J. S., and Richardson, D. C. (1999) *J. Mol. Biol. 285*, 1735−1747.
45. Richardson, D. C., and Richardson, J. S. (1994) *Trends Biochem. Sci. 19*, 135−138.

BI015871F